ORIGINAL PAPER

An improved ANFIS model predictive current control approach for minimizing torque and current ripples in PMSM-driven electric vehicle

Brijendra Sangar[1] · Madhusudan Singh[1] · Mini Sreejeth[1]

Abstract

Electric Vehicles (EVs) are anticipated to dominate passenger car transportation, playing a pivotal role in advancing sustainable mobility. However, with the increasing enthusiasm for EVs, impediments endure within the realm of power transmission. This is especially evident in addressing challenges related to minimizing torque ripple and implementing advanced control techniques in traction for high-performance and efficient operation of EVs. Numerous control algorithms for motor drives have been developed in the recent past but face challenges in attaining effective control under varying drive cycles of EVs. To tackle these challenges, motor drive control algorithms integrate various control techniques, including field orientation control, model predictive control, intelligent control, etc. This paper proposes an innovative online-tuned MPCC algorithm based on the adaptive neuro-fuzzy inference system (ANFIS). The traditional proportional–integral (PI) controller is replaced with an adapted ANFIS algorithm, and the tuning of ANFIS parameters is achieved by leveraging the error between the reference and adjustable models through a hybrid training algorithm. The proposed novel control technique improves the dynamic speed response of permanent magnet synchronous motor drives EVs. This improvement is realized by replacing the PI-HCC controller with an ANFIS controller coupled with MPCC. A laboratory prototype of the proposed control technique for EVs has been developed, and a comparative analysis of ANFIS-MPCC techniques with other known control techniques has been presented. This paper also demonstrates the importance of choosing optimal motor control techniques for torque ripple minimization and improving the overall performance of EVs.

1 Introduction

The PMSMs are now commonly used motors in electric cars due to their high torque-to-current and power-to-weight ratios, resulting in reduced physical size. PMSMs are light in weight, robust and require minimal maintenance with better dynamic performance due to the presence of a permanent magnet rotor [1]. These motors have a wide range of appli-cations, including EVs, medical applications, aeronautics, robotics, rail transport, energy conversion systems, etc. [2]. However, it is crucial to recognize the significant challenges associated with controlling these motors due to their non-linear and multivariable complex mathematical models. The presence of uncertainties in model parameters, such as the coefficient of friction, further complicates its control mecha-nism by introducing inherent uncertainties within the system [3].

The motor used for EV application may encounter various limitations, encompassing electrical, mechanical, magnetic, thermal, residual and environmental constraints [4]. In the quest for optimal performance, superior control, flexible operation, fast transient response and the mitigation of uncertainty-related challenges, several control methods have been developed in recent years. The exploration of control strategies for drives powered by power electronics converters represents a diverse field of applications.

✉ Brijendra Sangar
   brijendra_2k21phdee30@dtu.ac.in

   Madhusudan Singh
   madhusudan@dce.ac.in

   Mini Sreejeth
   minisreejeth@dce.ac.in

1 Department of Electrical Engineering, Centre of Excellence for EVRT, Delhi Technological University, Delhi 110042, India

The controllable parameters of a motor include speed, position, torque, power and other relevant factors. Several well-established decoupled control techniques, such as FOC, sliding mode control, direct power control (DPC), direct torque control (DTC), active disturbance rejection control, back-stepping control, input–output linearization control, neuro-fuzzy control and iterative learning control, have been extensively reported [5–7] for high-performance drives.

Recent advancements in high-performance electric drives using PMSM have given rise to advanced control approaches. The contemporary integration of "predictive control" in power converters powering electrical drives aims to elevate the efficiency of motor drive and control systems. Significantly, this control methodology has been gainfully utilized to tackle complex multivariate constrained control challenges in motor drives [8, 9].

The evolution of digital signal processors (DSPs) has facilitated the utilization of predictive control methodologies for motion control. Recently, predictive control has surfaced as a resilient controller suitable for a variety of systems, such as power electronic converters, motor drives and other applications. The fundamental idea behind predictive control involves utilizing the system model to predict the future behavior of control variables and then optimizing actions according to specified criteria [10]. Predictive control (PC) schemes can be classified into five categories: MPC, Deadbeat PC, trajectory-based PC, hysteresis-based PC and alternative techniques with diverse optimal decision-making criteria [11, 12].

The Deadbeat PC method employs the system model to determine the control variable that eliminates the error between the actual value of control variables and reference value. While it achieves excellent dynamic response, its effectiveness declines in the presence of variations and disturbances. Additionally, addressing system nonlinearities and constraints present challenges in implementation [13]. PC strategies centered on hysteresis and trajectory do not incorporate a modulation block and explicitly introduce switching states to the converter.

MPC is acknowledged as a straightforward and efficient control methodology for power converters and electric motor drives, and MPC has advantages in uncomplicated implementation in multivariate systems, acknowledgment of nonlinearities/constraints and commendable dynamics. MPC utilizes a mathematical model to forecast system behavior and minimizes a predefined cost function to attain the necessary control objectives [14]. MPC strategies can be classified into finite control set model predictive control (FCS-MPC) and continuous control set MPC (CCS-MPC). The CCS-MPC excels in seamlessly integrating nonlinearities/constraints and maintaining a consistent switching frequency. However, executing the entire control system in real time using a basic hardware platform is difficult.

It is important to understand how changes in parameters and outside disturbances affect FCS-MPC in complex driving environments. When parameters change or outside factors interfere, it can disturb the control system, making it less effective. For example, change in resistance and inductance can effect the control algorithms. To deal with these challenges, strong control methods, techniques that can adapt and find ways to spot and fix problems early, must be used [15]. Ultimately, making sure the control system works well in tough situations is a big deal, and it takes smart planning and design.

FCS-MPC reduces computational optimization time by utilizing a restricted number of switching states, rendering it easily implementable with straightforward hardware. FCS-MPC provides superior performance, rapid response and the capacity to manage numerous variables and constraints, thereby optimizing system behavior [16].

Despite its benefits, FCS-MPC faces constraints that impede its adoption in drive system [17]. The utilization of a solitary voltage vector (VV) within a single control period results in a conspicuous steady-state ripple. While elevating the sampling frequency enhances steady-state performance, it imposes a substantial computational load [18].

Hence, enhancing the steady-state performance without increasing the sampling frequency of the FCS-MPC algorithm is crucial [19]. This concern has been addressed in the proposed novel adaptive neuro-fuzzy inference system-based model predictive current control (ANFIS-MPCC) strategy. The proposed approach utilizes the motor as the reference model, employing the current model in the rotor reference frame as an adaptive model. This strategy replaces the conventional PI adaptation mechanism with an ANFIS-based alternative, as depicted in Fig. 1. The inputs for adjusting the adaptive model include the estimated direct and quadrature axes currents (i_d, i_q) and the motor's electrical angular velocity (ω_r). The error between the quadrature axes currents (i_q) from both models is employed for tuning ANFIS parameters. The proposed method contributes to the reduction of torque ripple during steady-state operation through

Fig. 1 Proposed ANFIS-MPCC PMSM drive's block diagram

precise and seamless current regulation. Consequently, this enhances motor efficiency and alleviates mechanical strain on the PMSM drive mechanism. Furthermore, ANFIS hysteresis current control generally presents a simpler and more direct control approach compared to the multivector scheme for steady-state operation [20]. This simplicity streamlines the implementation and adjustment of control parameters, thus mitigating the complexity of the control system. The proposed novel ANFIS adaptation mechanism requires reduced computational power by incorporation of a hybrid learning algorithm which facilitates expedited convergence rates. Specifically, the ANFIS adaptation mechanism proficiently handles the nonlinearities and parameter variations intrinsic to the PMSM drive.

The novelty of the proposed controller and the authors' contributions can be encapsulated as follows:

(1) Implementation of innovative speed controller for EV drive applications, based on ANFIS-MPCC. This controller exhibits superior control and tracking capabilities under diverse operating conditions.

(2) Comparative analysis of the dynamic performance of developed laboratory PMSM drive-based prototype under different operating condition using the proposed ANFIS-MPCC with other control techniques. Comparative analysis of the dynamic performance of developed laboratory PMSM drive-based prototype under different operating conditions using the proposed ANFIS-MPCC with other control techniques. A reduction of 64% in torque ripples, 70 % in current ripples and 52% in phase current harmonics was achieved with the proposed method as compared to the traditional method PI-HCC

(3) To assess the effectiveness of the proposed controller under typical vehicular circumstances, several tests have been conducted, including dynamic performance evaluation, load simulation, and efficiency and range assessment. The Modified Indian Drive Cycle (MIDC), designed to encompass a wider range of speed profiles, has been employed to evaluate the performance of the proposed ANFIS-MPCC. These tests revealed a 10% energy savings compared to conventional method.

This paper is structured into six sections, inclusive of the introduction. Section 2 is dedicated to the modeling of EV and PMSM. The control scheme is discussed in Sect. 4. Sections 4 and 5 present the simulation studies and experimental results and discussions, respectively, culminating in the conclusion presented in Sect. 6.

2 Mathematical modeling

2.1 Mathematical modeling of PMSM-based EV

It is imperative for every EV to exhibit performance characteristics that ensure safe integration with regular urban traffic. To achieve this, a comprehensive understanding of the various forces influencing the dynamics of an EV is essential. This section aims to elucidate each of these forces, ultimately synthesizing their contributions to derive an expression for the total force that must be overcome. This total force signifies the effort required by the PMSM to induce the linear movement of the electric vehicle [21]. Figures 2 and 3 offer a graphical depiction of the forces influencing the dynamics of the vehicle. Table 1 presents the vehicle parameters.

(a) Rolling resistance force The force of rolling resistance primarily arises due to the friction between the tire and the ground. This force remains relatively constant and is directly proportional to the total weight of the vehicle. The mathematical representation of this force is given by:

$$F_{\mathrm{rr}} = \mu_{\mathrm{rr}} mg \tag{1}$$

where μ_{rr} is the coefficient of rolling resistance, m is vehicle mass in kg and g is acceleration due to gravity.

(b) Aerodynamic drag force The aerodynamic drag force originates from the air resistance experienced by the moving vehicle body and is dependent on the frontal area. The equation governing this force is formulated as follows:

$$F_{\mathrm{ad}} = \frac{1}{2} \rho A C_{\mathrm{d}} v^2 \tag{2}$$

where ρ represents the air density in kg/m^3, A stands for the frontal area m^2, v in m/s denotes the speed of the vehicle and C_{d}, known as the drag coefficient, decreases its value, enhancing the aerodynamics of the vehicle

(c) Hill climbing force The force needed to drive the vehicle uphill on a slope ψ, designated as F_{hc} is essentially the weight of the vehicle component acting parallel to the incline. By analyzing the forces, it can be represented as illustrated in Fig. 2.

$$F_{\mathrm{hc}} = mg \sin \psi \tag{3}$$

(d) Acceleration force When the vehicle speed changes, an additional force beyond that depicted in Fig. 2 is necessary. This force, F_{la}, induces the linear acceleration of the vehicle and is described by Newton's second law equation,

$$F_{\mathrm{la}} = ma \tag{4}$$

Both angular acceleration of the vehicle's rotating elements and linear acceleration must be considered.
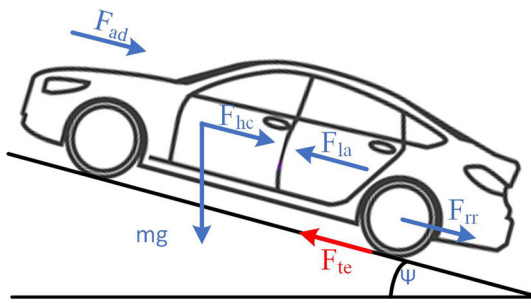
Fig. 2 Forces acting on the vehicle

Fig. 3 Motor gear arrangement

Figure 2 illustrates a simple method of connecting the PMSM with the traction wheels. The angular force required is:

$$F_{\omega a} = I \frac{G^2}{\eta_g r^2} a \tag{5}$$

The angular force required is linked to the motor transmission ratio (G), moment of inertia (I) of the motor's rotor, gear efficiency (η_g) and the radius (r) of the drive wheels. This relationship is expressed as follows: for: $\omega < \omega_c$, ov $< rG\omega_c$, then $T_L = T_{max}$ where:

$$F_{te} = \frac{G}{r} T \tag{6}$$

$$F_{te} = \mu_{rr} mg + \rho A C_d v^2 + ma + I \frac{G^2}{\eta_g r^2} a \tag{7}$$

then substituting (6) in (7), we have:

$$T_L = \mu_{rr} mg + \frac{\rho}{2} A C_d \omega^2 \frac{r^3}{G^3} + \left(m \frac{r}{G} + I \frac{G}{\eta_g r} \right) \dot{\omega} \frac{r}{G} \tag{8}$$

Considering that the Torque equation of the PMSM is:

$$J \dot{\omega} = T_e - T_L \tag{9}$$

substituting (8) in (9):

$$\dot{\omega} = \frac{T_e - \left(\mu_{rr} mg \frac{r}{G} + \frac{a}{2} A c_{\alpha^2} \omega^2 \frac{r^3}{c^2} \right)}{1 + \left(m \frac{r^2}{c^2} + \frac{1}{v_0} \right)} \tag{10}$$

The linear velocity v is obtained as:

$$\frac{dv}{dt} = \frac{T_e - \left(\mu_{rr} mg \frac{r}{G} + \frac{\rho}{2} A C_d \omega^2 \frac{r^3}{G^3} \right)}{J + \left(m \frac{r^2}{G^2} + \frac{\rho}{\eta_g} \right)} \tag{11}$$

Table 1 Vehicle parameters

Parameters	Symbols	Value	Unit
Vehicle mass	m	1.0	Per unit
Vehicle frontal area	A	235	m^2
Wheel rolling radius	r	0.3048	m
Gear ratio	G	2.5	–
Rolling resistance coefficient	μ_{rr}	0.015	–
Wind resistance coefficient	C_d	03	–

2.2 Modeling of PMSM and inverter

The assumption posits the neglect of motor core saturation, excluding both hysteresis losses and eddy current in the motor. Additionally, the rotor is presumed to be undamped. In the $d - q$ coordinate system, the surface PMSM stator voltage equation is [22] expressed as

$$\begin{cases} u_{sd} = R_s i_{sd} + \frac{d\psi_{sd}}{dt} - \omega_r \psi_{sq} \\ u_{sq} = R_s i_{sq} + \frac{d\varphi_{sq}}{dt} + \omega_r \psi_{sd} \end{cases} \tag{12}$$

The stator's electromagnetic equation is formulated as

$$\begin{cases} \psi_{sd} = L_{sd} i_{sd} + \psi_f \\ \psi_{sq} = L_{sq} i_{sq} \\ |\psi_s| = \sqrt{\psi_{sd}^2 + \psi_{sq}^2} \\ \delta = \arctan \left(\frac{\varphi_{sq}}{\psi_{sid}} \right) \end{cases} \tag{13}$$

The equation for electromagnetic torque is articulated as

$$T_e = \frac{3 p_\pi}{4 L_{sid} L_{xp}} |\psi_s| \left[2 \psi_f L_{sq} \sin \delta \right] \tag{14}$$

where R_s is stator resistance; T_e is electromagnetic torque; $|\Psi_s|$ is flux amplitude; ω_r is electrical angular velocity; P_n is number of pole pairs; u_{sd}, u_{sq} are stator voltages; $i_{s\phi} i_{sq}$ are stator currents; Ψ_f is permanent magnet flux; δ is load angle Ψ_{sd} and Ψ_{sq} are stator direct and quadrature magnet flux; and L_{sd} and L_{sq} are direct axis and quadrature axis inductance.

For a two-level three-phase inverter, switching signals under ideal condition for each phase Sa, Sb, Sc as follows $Sx(x = a, b, c)$.

$$S_x = \begin{cases} 0 & \text{if lower switch is on and upper switch is off} \\ 1 & \text{if upper switch is on and lower switch is off} \end{cases} \tag{15}$$

Hence, the two states for each phase can be consolidated into eight switching states, encompassing six nonzero vector states and two zero vector states, as shown in Fig. 1.

The output voltage vector in three phases is specified based on the inverter's switching state, as follows,

$$\begin{bmatrix} u_a \\ u_b \\ u_c \end{bmatrix} = \frac{v_{\text{dc}}}{3} \begin{bmatrix} 2 & -1 & -1 \\ -1 & 2 & -1 \\ -1 & -1 & 2 \end{bmatrix} \begin{bmatrix} S_a \\ S_b \\ S_c \end{bmatrix} \tag{16}$$

where $ux(x = a, b, c)$ represent phase voltages and V_{dc} is the DC bus voltage of inverter. The voltage vector on the dq axis is:

$$\begin{bmatrix} u_d \\ u_q \end{bmatrix} = \frac{2}{3} \begin{bmatrix} \cos\theta & \cos(\theta - 120°) & \cos(\theta + 120°) \\ -\sin\theta & -\sin(\theta - 120°) & -\sin(\theta + 120°) \end{bmatrix}$$
$$\times \begin{bmatrix} u_a \\ u_b \\ u_c \end{bmatrix} \tag{17}$$

3 ANFIS-MPCC controller for EV

3.1 Adaptive neuro-fuzzy inference system

ANFIS stands as a hybrid artificial intelligence paradigm that seamlessly integrates fuzzy logic and artificial neural networks for the purpose of acquiring a mapping input–output data, [23]. The holistic design of an ANFIS system, elucidated as shown Fig. 4, encompasses the subsequent components:
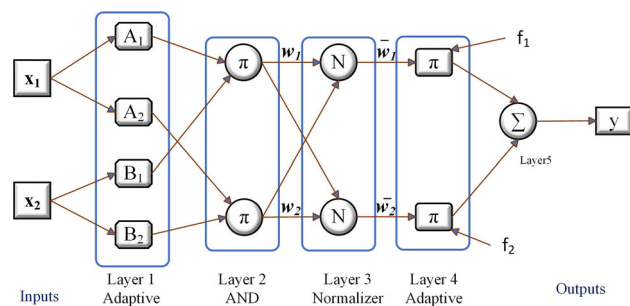
Layer 1: This layer assimilates fuzzy clusters from input data through the utilization of membership functions, articulated as:

$$O_i^1 = \mu_{A_i}(x) \tag{18}$$

In this equation, μ is the membership function, x represents the input to node i, $and A_i$ indicates the linguistic label of the node function.

Layer 2: The rule layer determines strengths by multiplying the membership values obtained from the fuzzification layer:

$$O_i^2 = w_i = A_i(x) \times B_i(y) \tag{19}$$

- Layer 3: This layer calculates normalized strengths associated with each rule through the following formula:

$$O_i^3 = \bar{w}_i = \frac{w_i}{\sum_i^n w_i} \tag{20}$$

where $\overline{w}_i$ is the normalized strength and n is the number of nodes.

Layer 4: The defuzzification layer determines weighted values of rules using first-order polynomials:

$$O_i^4 = \bar{w}_i f_i = \bar{w}_i (p_i x + q_i y + r_i) \tag{21}$$

In this context, f_i constitutes the polynomial incorporating the parameter set $\{p_i, q_i, r_i\}$ identified as consequence parameters.

Layer 5: This layer consolidates all outputs from the defuzzification layer, yielding the ANFIS output:

$$y = O_i^5 = \frac{\sum_i \omega_i f_t}{\sum_i \omega_i} \tag{22}$$

The structured architecture of the ANFIS system, encompassing these layers, enables effective learning and interpretation of intricate mappings from input to output as guided

Fig. 4 ANFIS architecture
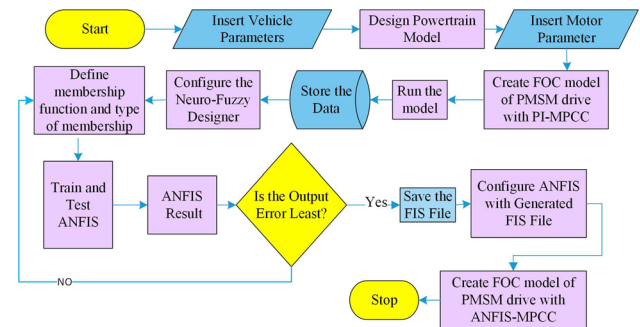
Fig. 5 Flowchart of ANFIS training methodology

Algorithm 1 ANFIS Training model

1: Define the vehicle and motor input parameters
2: Create FOC model for PMSM drive with PI-MPCC
3: Divide the dataset into training and testing set
4: Define the ANFIS architecture
5: Train the ANFIS model using a neural network
6: Evaluate the trained model
7: Use the trained ANFIS model for PMSM control

by the provided dataset and is shown through a flowchart as given in Fig. 5.

3.2 Model predictive current control

Following the fundamental tenet of predictive control, the Euler algorithm [24] is employed to discretize equation (23). Here, T_s denotes the sampling period, and the current at time $(k + 1)$ is predicted on the measurement available at time (k). The resulting discrete linear time-invariant system is:

$$\begin{cases} i_{sd}(k+1) = \left(1 - \frac{R_s T_s}{L_{sd}}\right) i_{sd}(k) + \omega_r T_s \\ \frac{L_{sq}}{L_{sd}} i_{sq}(k) + \frac{T_s}{L_d} u_d^*(k) \\ i_{sq}(k+1) = \left(1 - \frac{R_s T_s}{L_{sq}}\right) i_{sq}(k) - \omega_r T_s \\ \frac{L_{sq}}{L_{sd}} i_{sd}(k) + \frac{T_s}{L_d} u_q^*(k) - \omega_r T_s \frac{\psi_f}{L_q} \end{cases} \quad (23)$$

Due to the extensive computational requirements of the MPC control scheme, there is an inherent delay in its execution [25]. Failure to address this delay issue can impede the controller's ongoing operations, potentially resulting in a decline in control performance. Consequently, it is imperative to account for time delay compensation. Time delay compensation represents a straightforward and effective computational approach, wherein prediction control involves forecasting future values to serve as delay compensation. This approach is applied to current predictions to mitigate the impact of delays in the control process. The delay compensation algorithm is for forecasting the value at time k + 2, with the available information at time k, where $u_d^*(k)$ and $u_d(k)$ represent the applied voltage vectors.

$$\begin{cases} i_{sd}(k+2) = \left(1 - \frac{R_s T_s}{L_{sd}}\right) i_{sd}(k+1) + \omega_r T_s \\ \frac{L_{sq}}{L_{sd}} i_{sq}(k+1) + \frac{T_s}{L_{dd}} u_d^*(k) \\ i_{sq}(k+2) = \left(1 - \frac{R_s T_s}{L_{sq}}\right) i_{sq}(k+1) - \omega_r T_s \\ \frac{L_{sq}}{L_{sd}} i_{sd}(k+1) + \frac{T_s}{L_{dd}} u_q^*(k) - \omega_r T_s \frac{\psi_f}{L_q} \end{cases} \quad (24)$$

The control objectives of FCS-MPC algorithms are articulated through a cost function, serving as an indicator of the extent to which each switching state of the inverter achieves the desired system behavior. Specifically, in the context of current control, where the aim is to follow a reference cur-

Table 2 PMSM parameters

Parameters	Symbol	Value	Unit
Stall torque	Ts	8	Nm
Peak torque	T	24	Nm
Rated speed	ω_r	3000	rpm
Rated voltage	V	380	V
No. of poles	P_n	6	–
Stator resistance	R	0.95	ohm
Rated current	I	5.4	A
Inductance	Ls	8.2	mH
Inertia	J	00.15	$kg - m^2$
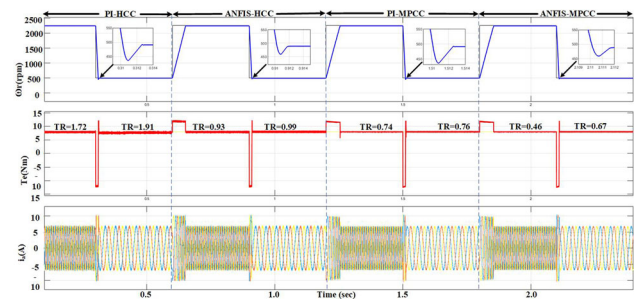
Fig. 6 Dynamic response while speed changes from 2250 to 500 rpm at 8 Nm load
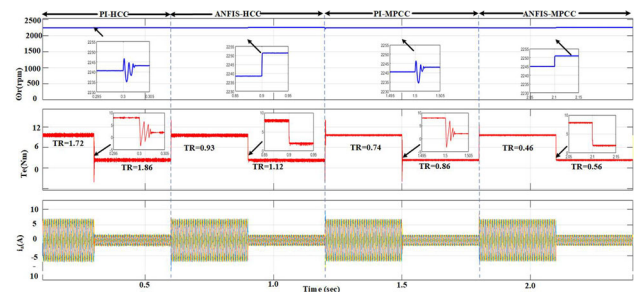
Fig. 7 Dynamic response while load changes from 8 to 2 Nm at 2250 rpm

rent (i_{sd}^*, i_{sq}^*) with predicted components (i_{sd}, i_{sq}), the cost function is precisely defined as

$$g = |i_{sd}^*(k+2) - i_{sd}(k+2)|^2 + |i_{sq}^*(k+2) - i_{sq}(k+2)|^2 \quad (25)$$

4 Simulation results and discussion

This section describes the simulations studies on a 2-kW PMSM with parameters as shown in Table 2. To assess the efficacy of the proposed novel ANFIS-MPCC technique, simulation model is developed in MATLAB/SIMULINK and also a prototype laboratory setup to validate the sim-

Table 3 Comparative results of torque ripples

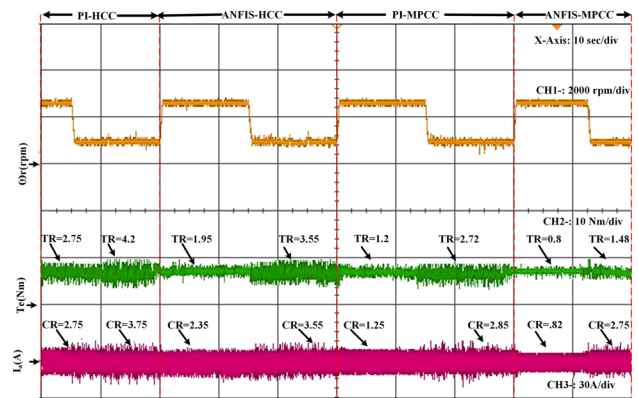| Control scheme	PI-HCC Simulation	PI-HCC Experimental	ANFIS-HCC Simulation	ANFIS-HCC Experimental	PI-MPCC Simulation	PI-MPCC Experimental	ANFIS-MPCC Simulation	ANFIS-MPCC Experimental
2250 rpm, 8 Nm (Nm)	1.72	2.75	0.93	1.95	0.74	1.2	0.46	0.8
500 rpm, 8 Nm (Nm)	1.91	4.2	0.99	3.55	0.76	2.72	0.67	1.48
2250 rpm, 2 Nm (Nm)	1.86	3.97	1.12	3.5	0.86	2.8	0.56	1.45
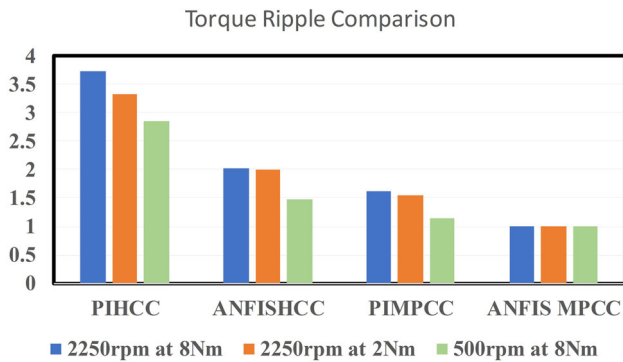
Fig. 8 Comparative simulation analysis of normalized torque ripple
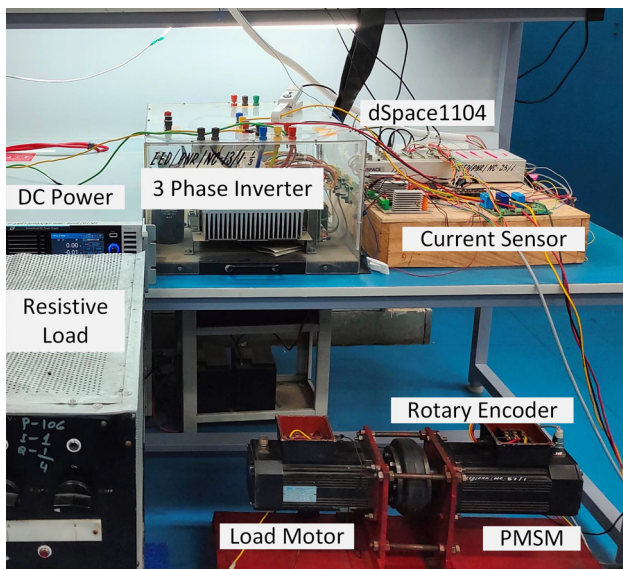
Fig. 9 Laboratory prototype for testing the ANFIS-MPCC-based PMSM drive

Fig. 10 Dynamic response for step speed change from 2250 to 500 rpm at 8 Nm load
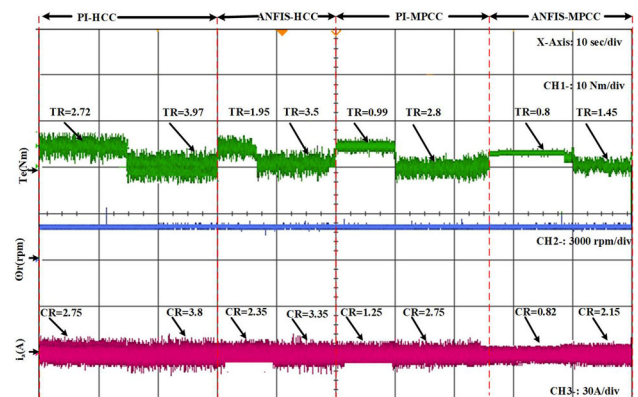
Fig. 11 Dynamic response for step load change from 8 to 2 Nm at 2250 rpm

ulated results. This study describes comparative simulations conducted on a 2-kW PMSM to assess the efficacy of the proposed method. The simulation commences with an initial speed of 2250 rpm (75% of the rated speed) and a load torque of 8 Nm (100% of the rated load) as shown in Fig. 6. In the time interval from 0 to 0.6 s, the PI-HCC algorithm is utilized, followed by the execution of ANFIS-HCC from 0.6 to 1.2 s. Subsequently, PI-MPCC is implemented from 1.2 to 1.8 s, and the proposed algorithm is activated from 1.8 to 2.4 s. Upon a sudden reduction in the speed com-

mand from 2250 to 500 rpm, the motor speed closely tracks the reference speed. The proposed ANFIS-MPCC exhibits a slightly reduced torque ripple (TR) of 73.2% (PI-HCC), 50.5% (ANFIS-HCC) and 37.8% (PI-MPCC) at 2250 rpm. At 500 rpm, ANFIS-MPCC yields a lower torque ripple of 64.9% (PI-HCC), 32.3% (ANFIS-HCC) and 11.8% (PI-MPCC).

Similarly, in the event of a sudden reduction in load torque from 8 to 2 Nm, the speed controller sustains the constant speed at 2250 rpm, with a momentary speed dip illustrated in Fig. 7. Furthermore, at 100% of full load, it is observed that ANFIS-MPCC exhibits a lower torque ripple compared to other control algorithms, as detailed in Table 3. The nor-
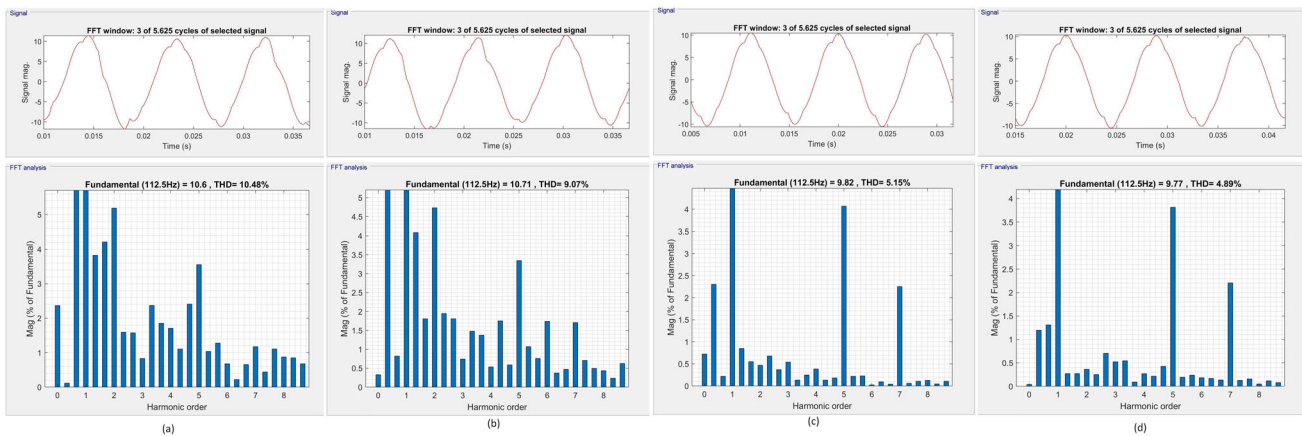
Fig. 12 Phase current harmonic analysis at 2250 rpm at 8 Nm load. **a** PI-HCC, **b** ANFIS-HCC, **c** PI-MPCC, **d** ANFIS-MPCC
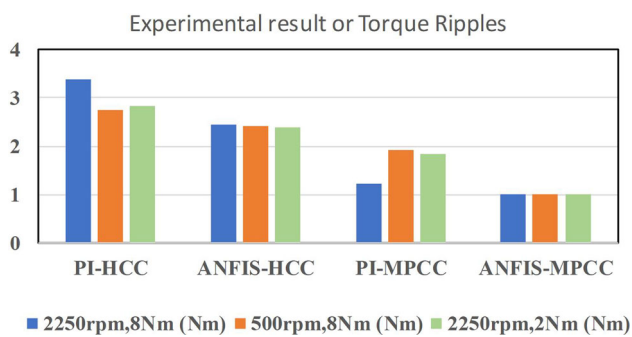

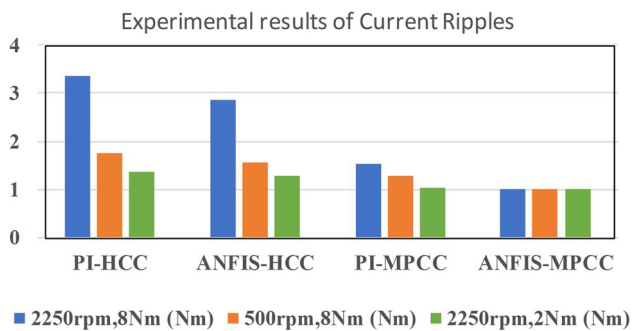**Fig. 13** Comparative analysis of normalized torque ripple

Fig. 14 Comparative analysis of normalized current ripple

malized comparative analysis is presented in Fig. 8 where proposed ANFIS-MPCC method TR is taken as reference 1.0

5 Experimental results and analysis

5.1 Experimental setup

This section describes comparative study of the theoretical and experimental results conducted on a 2-kW experimental setup featuring a PMSM to evaluate the efficacy of the proposed method. Experimental testing of the ANFIS-MPCC control scheme for a six-leg voltage source inverter (VSI) driving the PMSM was carried out and compared with traditional PI and HCC schemes. The laboratory prototype of the PMSM drive is shown in Fig. 9. The hardware implementation involves the utilization of a dSPACE controller DS1104 digital control board and a PMSM drive. Additionally, another PMSM functioning as a permanent magnet synchronous generator (PMSG) is coupled with PMSM to generate the necessary load torque. The inverter for the drive makes use of insulated gate bipolar transistors (IGBTs). Execution of all control algorithms takes place on the dSPACE controller (DS1104) digital control board through MATLAB program. Hall sensors are employed to measure the phase currents of the PMSM, while 1000 pulses per revolution incremental encoder is used to acquire the angular position and speed of the motor.

In each control approach, the PI controller parameters are tuned according to the Ziegler–Nichols method to attain optimal control performance. To facilitate a fair comparison, the speed PI controller maintains consistent parameters across all schemes, set as $K_p = 0.012$ and $K_i = 0.2$

5.2 Dynamic performance of PMSM drive

In this experimental setup, PMSM is initially started with a speed of 2250 rpm, representing 75% of the rated speed, and a load torque of 8 Nm, corresponding to 100% of the rated load. The PI-HCC algorithm is used in the time interval from 0 to 20 s, followed by the execution of ANFIS-HCC from 20.1 to 50 s. Subsequently, PI-MPCC is applied from 50.1 to 80 s, and the proposed algorithm is activated from 80.1 to 100 s as shown in Fig. 10. When the speed command undergoes

Table 4 Experimental results of current ripples

Control scheme	PI-HCC	ANFIS-HCC	PI-MPCC	ANFIS-MPCC
2250 rpm, 8 Nm (Nm)	2.75	2.35	1.25	0.82
500 rpm, 8 Nm (Nm)	3.75	3.55	2.85	2.75
2250 rpm, 2 Nm (Nm)	3.8	3.35	2.75	2.15
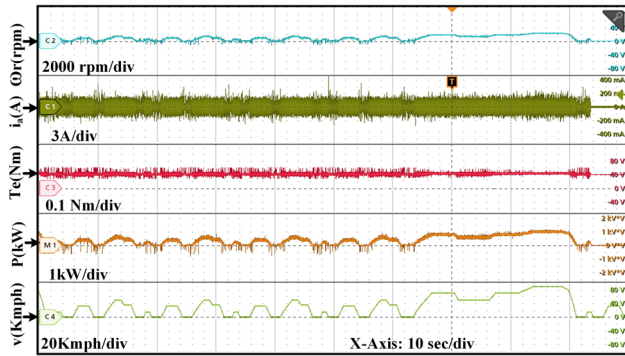
Fig. 15 Dynamic response of MIDC drive cycle

Fig. 16 Comparative analysis of energy consumption for MIDC cycle

an abrupt reduction from 2250 to 500 rpm, the motor speed closely adheres the reference speed. The proposed ANFIS-MPCC, as suggested, exhibits a significantly reduction in torque ripple of 70.9%, 58.9% and 33.3% in comparison with PI-HCC, ANFIS-HCC and PI-MPCC, respectively, at 2250 rpm. Likewise, at 500 rpm, the torque ripple is decreased by 64.7%, 58.3% and 45.5% when compared to the corresponding control strategies mentioned above as delineated in Table 3.

Similarly, in the case of an abrupt decrease in load torque from 8 to 2 Nm, the speed controller sustains at steady state speed at 2250 rpm with a temporary dip in speed as shown in Fig. 11. Furthermore, under conditions of full load (100%), it is observed that ANFIS-MPCC exhibits a reduced torque and current ripples as compared to alternative control algorithms, as delineated in Table 3. Figure 12 shows the fast Fourier analysis of phase current at 2250 rpm with a mechanical load of 8 Nm. The proposed method shows 52.48%, 45.05%, and 3.3% reduction in harmonics as compared to PI-HCC, ANFIS-HCC and PI-MPCC, respectively. Comparative analysis of normalized torque and current ripples is presented in Figs. 13 and 14 where TR and CR of the proposed ANFIS-MPCC method are taken as reference "1." The proposed ANFIS-MPCC demonstrates diminished current ripple (CR) of 70.2%, 65.1%, and 36% as compared to PI-HCC, ANFIS-HCC, and PI-MPCC, respectively, at 2250 rpm. Similarly, at 500 rpm, there is a reduction in current ripple by 26.6%, 22.5%, and 3.1% in comparison with the respective aforementioned control strategies as shown in Table 4.
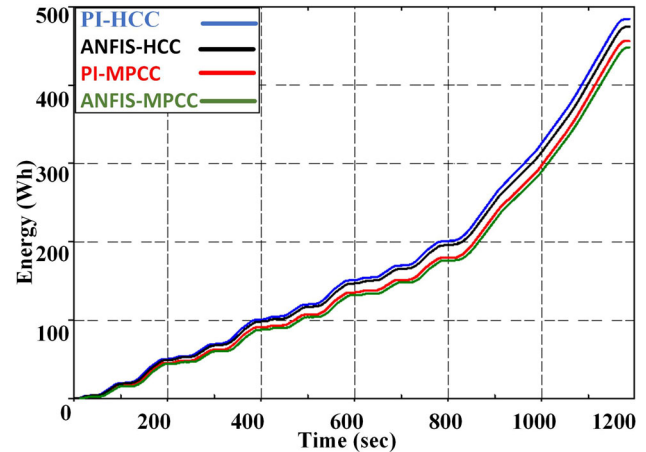
5.3 Performance validation using vehicular condition

For validating the vehicular conditions, the performance, reliability and safety of PMSM drive systems have been tested, thereby contributing to the development of more efficient and dependable electric propulsion solutions. The validation process includes dynamic performance evaluation, load simulation and efficiency and range assessment

5.3.1 Dynamic performance evaluation

This process entails assessing the motor's reactions across diverse driving scenarios, encompassing acceleration, deceleration and constant-speed operations. It includes analyses of torque output, speed responsiveness and current drawn under varied driving profiles to gauge the motor's dynamic characteristics and operational efficiency.

5.3.2 Load simulation

Load testing emulates a spectrum of vehicle loads and road conditions to gauge the motor's functionality under different stress levels. It aids in discerning the motor's performance under varied loads, including uphill driving, towing or carrying heavy payloads.

5.3.3 Efficiency and range assessment

The assessment of the motor's efficiency in real-world driving conditions is pivotal for understanding its impact on the vehicle's overall range and energy consumption. Efficiency testing entails the measurement of energy consumption at differing speeds, accelerations and driving modes to optimize the motor's functionality for maximum range.

A standard automotive drive cycle test is employed to validate the viability and robustness of the proposed ANFIS-MPCC technique for vehicular condition. The Modified Indian Drive Cycle (MIDC) is the modified form of NEDC (New European Drive Cycle) [26] designed for Indian traffic condition. The MIDC accounts for wider speed profiles is used to assess the performance of the proposed ANFIS-MPCC across a broad spectrum of speed changes. Such speed changes are very common in urban drive cycle and this drive cycle test is conducted at a constant load of 4 Nm and zero inclination. The dynamic performance of laboratory prototype with the suggested ANFIS-MPCC is tested with the MIDC. The motor speed (ω_r), electromagnetic torque (T_e), power (P) and current (I_a) are illustrated in Fig. 15

A comparative analysis of the energy consumption is also carried out for the traditional (PI-HCC, ANFIS-HCC and PI-MPCC) and proposed (ANFIS-MPCC) algorithms with MIDC and is shown in Fig. 16. It is observed that the proposed ANFIS-MPCC resulted in less energy consumption as compared to the other methods, thus validating that the proposed ANFIS-MPCC is best suited for EV applications.

6 Conclusion

This paper presents an innovative and simple approach for implementing ANFIS-MPCC in PMSM drive speed control. the proposed method utilizes and ANFIS-MPCC for PMSM drive speed control. Comparative assessments are carried out with traditional PI-HCC, ANFIS-HCC and PI-MPCC strategies. The simulation study and hardware implementation results reveal that substantial reduction in torque and current ripples is achieved using the proposed method as compared to conventional algorithms. Experimental validation of the ANFIS-MPCC using the MIDC illustrates substantial decrease in energy consumption. As compared to the conventional control algorithms for PMSM drive, the proposed ANFIS-MPCC controller offers several advantages as specified below:

(1) Under steady-state conditions, experimental findings show that the proposed ANFIS-MPCC-based controller can reduce motor torque ripples by 70.9%, 58.9% and 33.3% at high-speed operation as compared to PI-HCC, ANFIS-HCC and PI-MPCC, respectively. Further, at

low-speed operation the respective values are 64.7%, 58.3% and 45.5% as compared to PI-HCC, ANFIS-HCC and PI-MPCC, respectively.

(2) A smoother dynamic response to step change in speed is observed for the proposed ANFIS-MPCCC controller. It also exhibits lesser current ripples for both low-speed and high-speed operation as compared to other methods.

(3) The proposed method show better quality of power usage by reducing harmonics, 52.48%, 45.05% and 3.3% as compared to PI-HCC, ANFIS-HCC and PI-MPCC.

(4) There is significant reduction in energy consumption with the proposed ANFIS -MPCC method while testing using the MIDC drive cycle. The comparative analysis demonstrates a reduction of 10.2%, 6.7% and 2.6% of energy consumption as compared to PI-HCC, ANFIS-HCC and PI-MPCC, respectively, thus making the proposed ANFIS-MPCC-based PMSM drive for EV applications.

Both simulation studies and experimental results validate the effectiveness of the proposed approach over conventional methods in achieving enhanced steady-state and dynamic performances across diverse operational scenarios.

Declarations

Conflict of interest The authors declare no conflict of interest.

References

1. Wang Z, Ching TW, Huang S, Wang H, Xu T (2020) Challenges faced by electric vehicle motors and their solutions. IEEE Access 9:5228–5249

2. Lara J, Xu J, Chandra A (2016) Effects of rotor position error in the performance of field-oriented-controlled PMSM drives for electric vehicle traction applications. IEEE Trans Ind Electron 63(8):4738–4751

3. Yang J, Chen W-H, Li S, Guo L, Yan Y (2016) Disturbance/uncertainty estimation and attenuation techniques in PMSM drives: a survey. IEEE Trans Ind Electron 64(4):3273–3285

4. Hong J, Park S, Hyun D, Kang T-J, Lee SB, Kral C, Haumer A (2012) Detection and classification of rotor demagnetization and eccentricity faults for PM synchronous motors. IEEE Trans Ind Appl 48(3):923–932

5. Suryakant SM, Singh M, Seth AK (2023) Minimization of torque ripples in PMSM drive using PI-resonant controller-based model predictive control. Electr Eng 105(1):207–219

6. Dat NT, Van Kien C, Anh HPH (2023) Advanced adaptive neural sliding mode control applied in PMSM driving system. Electr Eng 105(5):3255–3262

7. Sreejeth M, Singh M, Kumar P (2015) Particle swarm optimisation in efficiency improvement of vector controlled surface mounted

permanent magnet synchronous motor drive. IET Power Electron 8(5):760–769

8. Schwenzer M, Ay M, Bergs T, Abel D (2021) Review on model predictive control: an engineering perspective. Int J Adv Manuf Technol 117(5–6):1327–1349

9. Shukla S, Sreejeth M, Singh M (2021) Minimization of ripples in stator current and torque of PMSM drive using advanced predictive current controller based on deadbeat control theory. J Power Electron 21:142–152

10. Cortés P, Kazmierkowski MP, Kennel RM, Quevedo DE, Rodríguez J (2008) Predictive control in power electronics and drives. IEEE Trans Ind Electron 55(12):4312–4324

11. Zhang Y, Ji C, You Q, Sun D, Xie Y (2023) Deadbeat predictive current control for surface-mounted permanent-magnet synchronous motor based on weakened integral sliding mode compensation. Appl Sci 13(21):11678

12. Wang J, Tang Y, Lin P, Liu X, Pou J (2019) Deadbeat predictive current control for modular multilevel converters with enhanced steady-state performance and stability. IEEE Trans Power Electron 35(7):6878–6894

13. Ramya L, Sivaprakasam A (2020) Application of model predictive control for reduced torque ripple in orthopaedic drilling using permanent magnet synchronous motor drive. Electr Eng 102(3):1469–1482

14. Karamanakos P, Liegmann E, Geyer T, Kennel R (2020) Model predictive control of power electronic systems: methods, results, and challenges. IEEE Open J Ind Appl 1:95–114

15. Li T, Sun X, Yao M, Guo D, Sun Y (2023) Improved finite control set model predictive current control for permanent magnet synchronous motor with sliding mode observer. IEEE Trans Transp Electrif. https://doi.org/10.1109/TTE.2023.3293510

16. Yu B, Song W, Yang K, Guo Y, Saeed MS (2021) A computationally efficient finite control set model predictive control for multiphase PMSM drives. IEEE Trans Ind Electron 69(12):12066–12076

17. Nguyen HT, Jung J-W (2018) Finite control set model predictive control to guarantee stability and robustness for surface-mounted PM synchronous motors. IEEE Trans Ind Electron 65(11):8510–8519

18. Liu X, Qiu L, Fang Y, Wang K, Li Y, Rodriguez J (2022) A fuzzy approximation for FCS-MPC in power converters. IEEE Trans Power Electron 37(8):9153–9163

19. Li T, Sun X, Lei G, Guo Y, Yang Z, Zhu J (2022) Finite-control-set model predictive control of permanent magnet synchronous motor drive systems: an overview. IEEE/CAA J Autom Sin 9(12):2087–2105

20. Sun X, Li T, Yao M, Lei G, Guo Y, Zhu J (2021) Improved finite-control-set model predictive control with virtual vectors for PMSHM drives. IEEE Trans Energy Convers 37(3):1885–1894

21. Larminie J, Lowry J (2012) Electric vehicle technology explained. John Wiley & Sons, Hoboken

22. Wu X, Zhang Y, Shen F, Yang M, Wu T, Huang S, Cui H (2023) Equivalent three-vector-based model predictive control with duty cycle reconstruction for PMSM. IEEE Trans Ind Electron 99:1–10

23. Shukla S, Sreejeth M, Singh M et al (2022) Improved ANFIS based MRAC observer for sensorless control of PMSM. J Intell Fuzzy Syst 42(2):1061–1073

24. Yang Y, Wen H, Li D (2017) A fast and fixed switching frequency model predictive control with delay compensation for three-phase inverters. IEEE Access 5:17904–17913

25. Han Y, Gong C, Yan L, Wen H, Wang Y, Shen K (2020) Multiobjective finite control set model predictive control using novel delay compensation technique for PMSM. IEEE Trans Power Electron 35(10):11193–11204

26. Ruuskanen V, Nerg J, Rilla M, Pyrhönen J (2016) Iron loss analysis of the permanent-magnet synchronous machine based on finite-element analysis over the electrical vehicle drive cycle. IEEE Trans Ind Electron 63(7):4129–4136